01NVSOQ – Advanced Antenna Engineering
Assignment 4: array components

Amedeo Bertone (243878)
Davide Botteon (239595)
Enrico Maria Renzi (244028)

January 18, 2018

Contents

1 Introduction

The goal of this project is the simulation of the complete structure realizing a four element array with amplitude tapering, obtaining a SLL of -20 dB.

The design is the same one we proposed in the previous assignment, but all the components will undergo a process of optimization in order to make us able to provide reliable and complete simulations finally attesting the correct behavior of the structure.

The first part will deal with the simulation and optimization of the power splitters that will later be inserted in the BFN. Both the even and uneven power splitter will be tested in order to identify the discontinuities present in the model and minimizing their effect.

The second part is related to the simulation of the BFN, in order to verify if the previously optimized splitters still work the right way when united in a single model and to correct the structure if not.

Last, in the third and final part, the complete antenna will be tested and its radiating properties will finally be verified, allowing us to finally understand

if the BFN feeds the structure in a way that fulfills the design requirements or not.

At the end of the three described phases, a cad file will be produced containing the information about the final structure a producer would need in order to print the antenna.

2 Sections fine tuning

Second T Regarding the optimization of the second T junction we used the T designed for the previous assignment and we connect to it the two lines routing to the patches. In this way we control also the contributions due to the discontinuities on all the second part of the beam forming network.

Simulating this new component we have that the matching is no more on the wanted frequency of $2.45GHz$ but some megahertz higher. In order to make it decrease at first we tried to change the values external to the T junction with a freedom degree, that in particular are the angle and the tapering of the bending. The results varying those values are showed in the graphs below. Notice that in practice the resonance is not moved in both the cases.

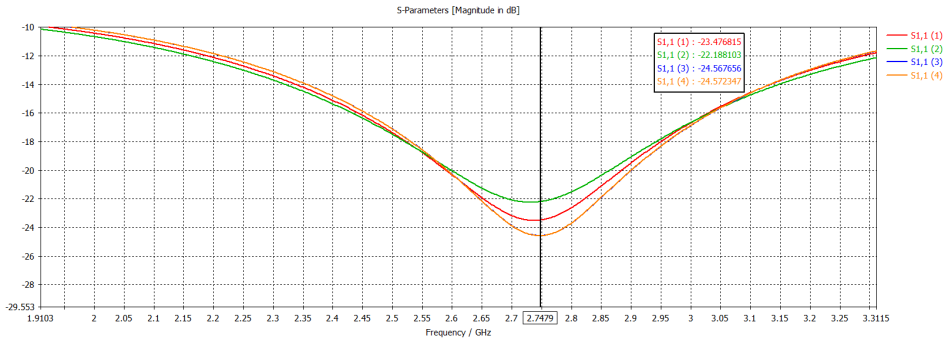

Figure 1: s11 with respect to the bend angle

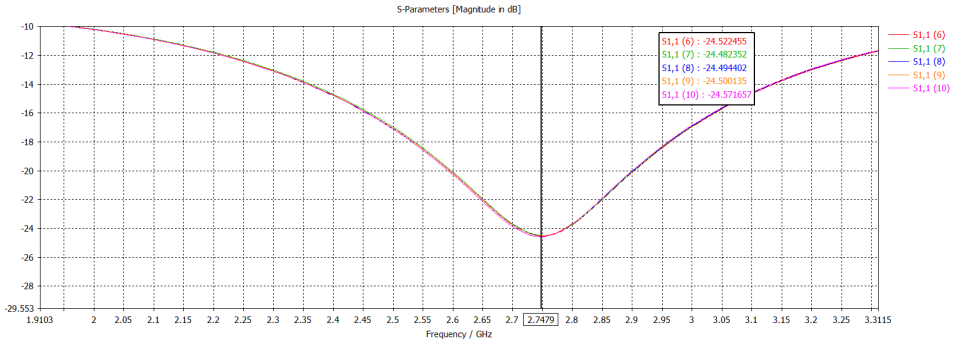

Figure 2: s11 with respect to the bend tapering

Now we have tried to not modify the T junction parameters, but since this way didn't produce the desired effect we have to change the the $\lambda/4$ impedance transformer's length. The graphs below shows the values obtained first with simply changing the transformer length and second the also re-using the old optimized value of the single T junction (notice that in the second case the return losses are lower).

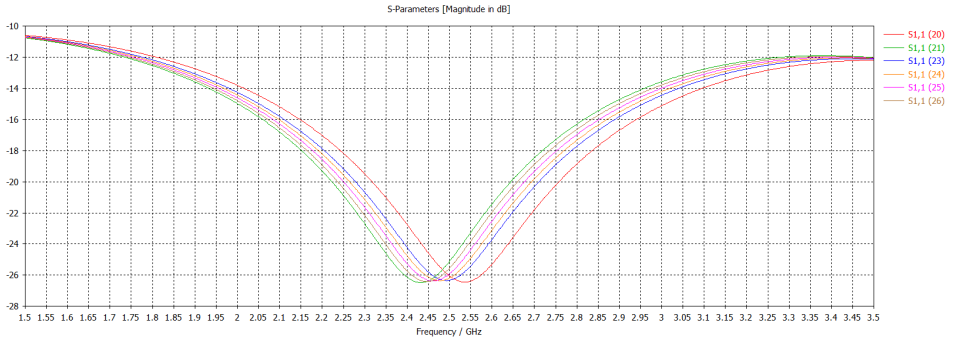

Figure 3: s11 with respect to the $\lambda/4$ transformer's length

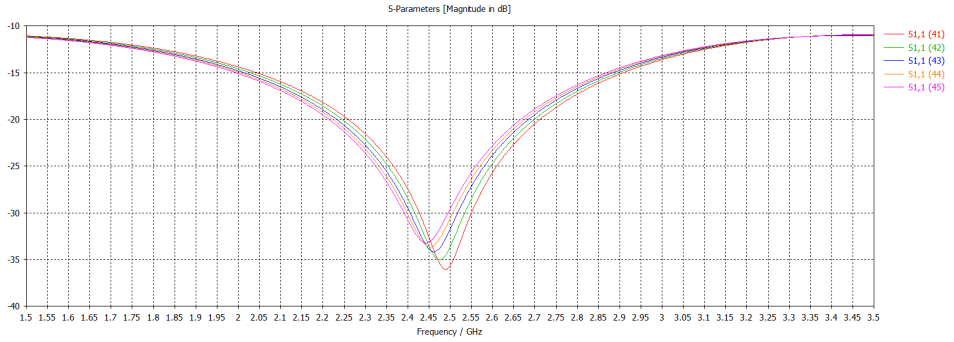

Figure 4: s11 with respect to the $\lambda/4$ transformer's length – changed values

With this final value we reached the desired behavior, so we can use this for composing the complete beam forming network. On the following figure is showed the result, notice that also the s_{21} and the s_{31} have the proper values in order to generate the desired tapering.

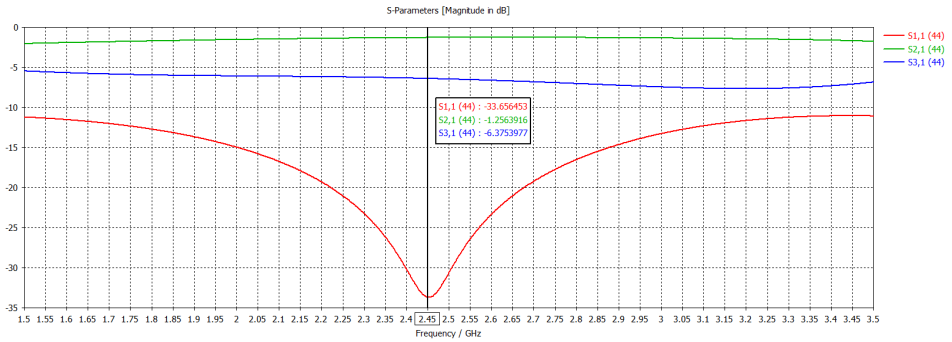

Figure 5

3 BFN fine tuning

Before proceeding with the simulation of the overall antenna we decided to perform an optimization of the BFN.

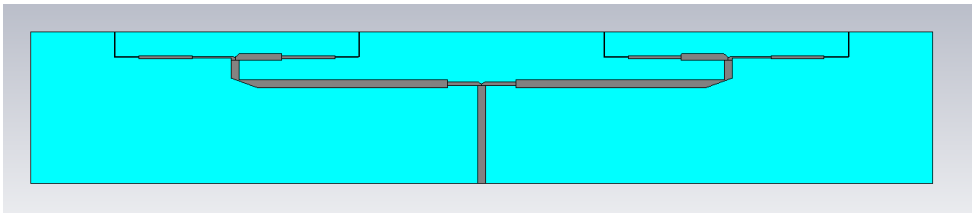

Figure 6: How the final BFN looks like

The attention was mainly focused on:

- tuning of the S_{11} parameter, in order to obtain a resonant behavior at 2.45 GHz
- achieving the best possible tapering, i.e. as close as possible to the theoretical value of 5.3 dB needed in order to get the right SLL in the final structure
- obtaining the right phasing between the elements, i.e. phase difference as close as possible to zero, since the array must be broadside.

Before showing the results of the simulations it is worth to spend a few words about meshes; in fact, as explained in class, the correct definition

of the meshgrid is fundamental in order to assure the correct behavior of the waveguide ports and a reliable analysis of all the discontinuities present inside the model. That being said, we decided to impose a refinement of the grid across the more sensitive areas (thin elements and discontinuities) and second, a symmetry plane, which allowed to reduce the simulation time thanks to the intrinsic symmetry of the structure. Figure 7 gives an idea of how thin the mesh was around the critical points, while figures 8 and 9 show exactly how the settings were manipulated in order to obtain it.

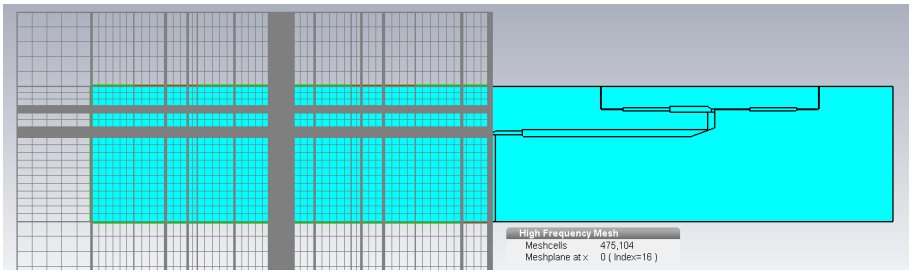

Figure 7: Mesh View of the BFN, showing the used symmetry plane setting too

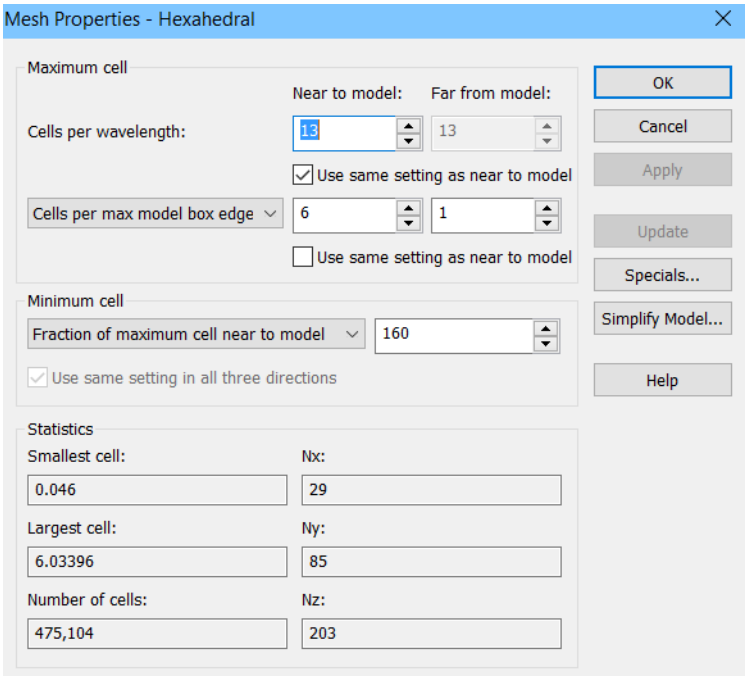

Figure 8: Imposed Mesh Properties

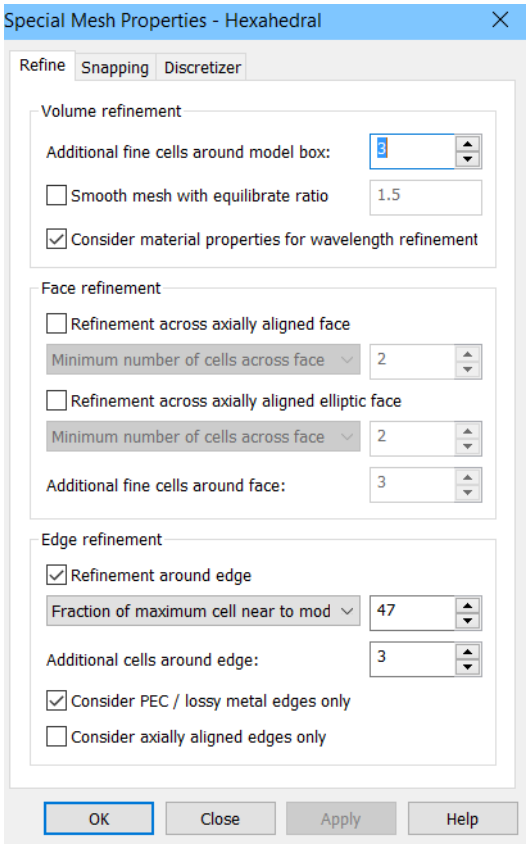

Figure 9: Imposed Special Mesh Properties

Now that we've concluded the discussion about adopted procedures (which obviously included a certain number of parametric sweeps and optimizer runs in order to refine the results) we can discuss the obtained parameters.

First, the S_{11} is shown, figure 10. The resonance point coincides almost exactly with 2.45 GHz and its level in dB is quite reassuring (-35 dB). It has to be said that we were able to obtain even lower values for our resonance (-45 dB), but in the end the shown solution was chosen because of its better behavior in terms of tapering and of the better results obtained when simulating it with the radiating elements.

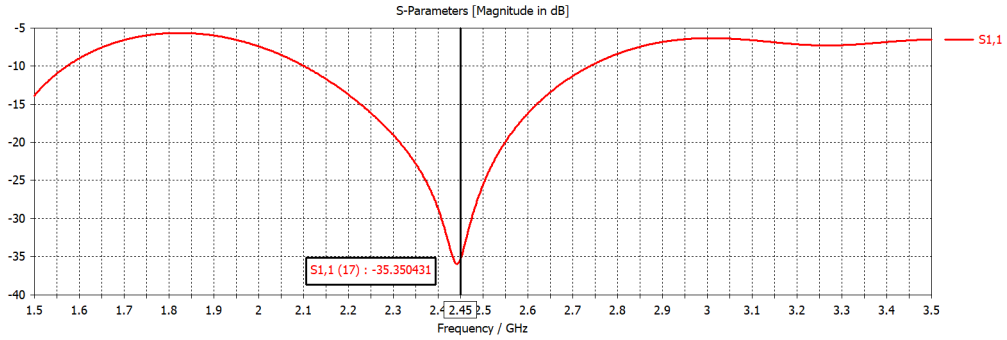

Figure 10: S_{11} parameter of our BFN

As figures 11 and 12 show, the tapering is around 5.05 dB while the phase difference between adjacent elements is lower than 1°.

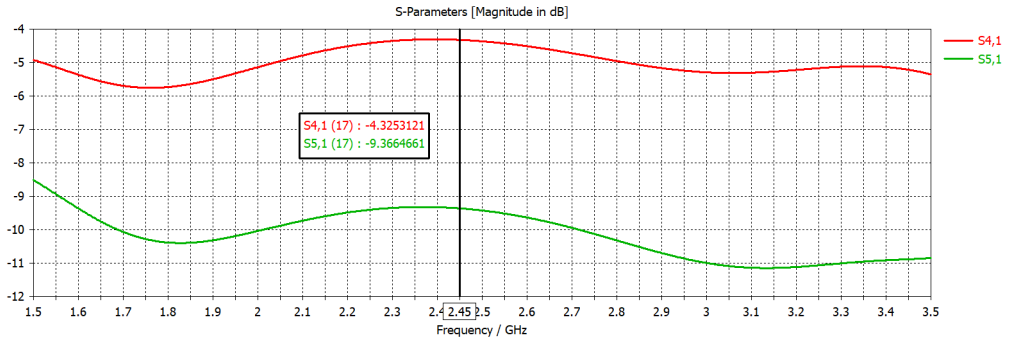

Figure 11: behavior in terms of tapering

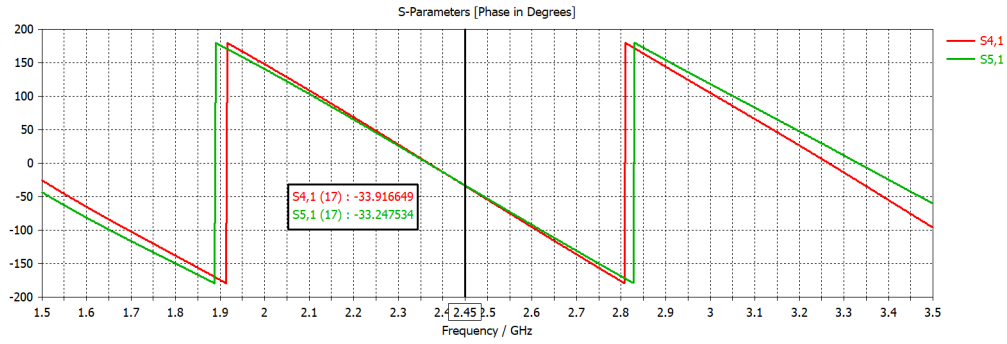

Figure 12: behavior in terms of phase

Last but not least, figure 13 shows an estimation of the -10 and -20 dB obtained bandwidths.

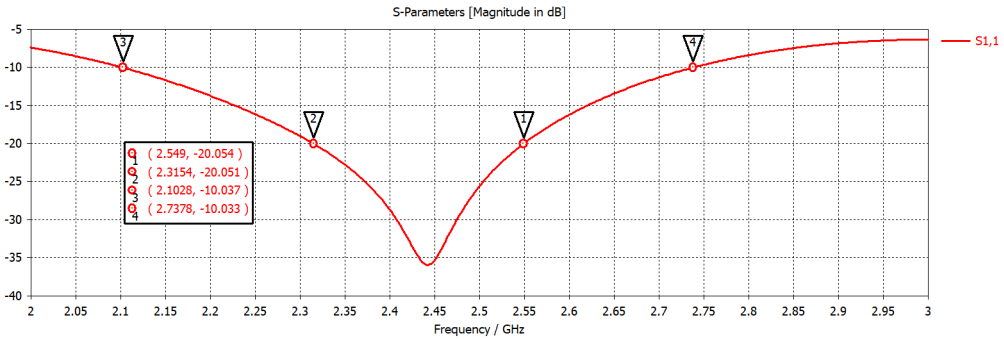

Figure 13: estimation of the bandwidth of the BFN

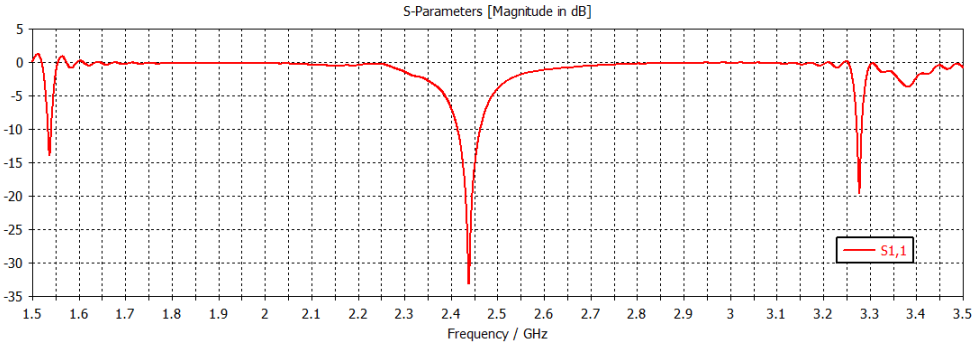

Figure 14: Broadband view for the input reflection coefficient seen from full array input port.

4 Full array fine tuning and results

Within this last step the tuned BFN and radiating part are connected. The spacing between elements is set to be compliant with the GL limit at the central resonance frequency f_0=2.45GHz (distance between elements, d=$\leq$88mm). Actually what follows mainly concerns the full antenna's radiation pattern, rather than the array factor alone. This is legitimated by the following facts:

- what can be measured to describe the real radiation properties of a microstrip array antenna is the far field radiation pattern;
- the full AF's extraction from simulation introduces numerical errors that makes the calculation inaccurate far from the main lobe centre.

Furthermore, moving the GL requirement from AF to the radiation patter, we gain a more robust design, less affected by discontinuities' and line width's losses[1].

Patch's width and length are set equal to: W_{patch}=64mm and L_{patch}=24.7mm. Once BFN and radiators have been joint, we have the complete array reported in figure 16, which has been simulated with the mesh settings printed in figure 17. To keep the computation simpler we exploited the microstrip field distribution and a (y,z) transverse magnetic field symmetry plane has been used as boundary condition (with open boundary, added space in all directions).

Finally, the simulation's outcomes are the following:

Return loss and bandwidth Overall, the input reflection coefficient is worsened by the connection of the two parts. Although the various

[1]the total radiation pattern is given by the product of the single patch's pattern and the normalized array factor. Since the former term damps the latter then the total radiated field will be lowered as well. Moreover we can relax the requirement on tapering having more uniform microstrip lines (in terms of width).

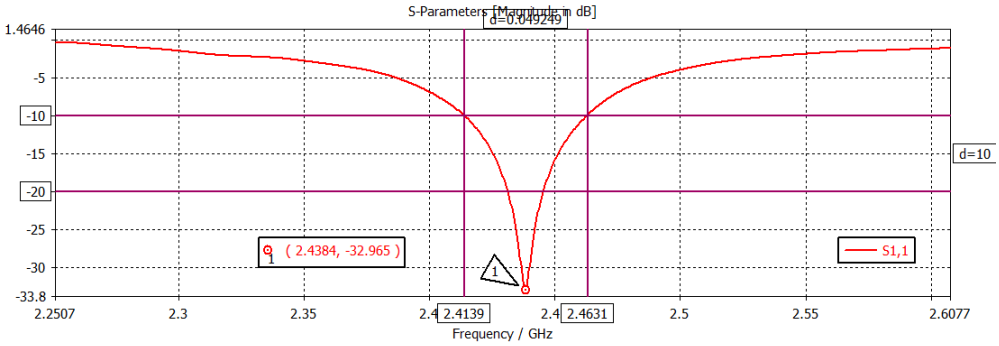

Figure 15: In-band view for the input reflection coefficient seen from full array input port.

sections have been finely tuned, the difference between using excitation ideal port and connecting actual transmission lines cannot be reduced further. We reported in figure 14 the best result allowed by optimization. Unfortunately $|S_{11}|$ reaches its minimum at f_0'=2.438GHz, not exactly at f_0=2.45GHz. Though we obtained such discrepancy, this should not be a problem because this simulation does not represents the real behaviour of the built antenna, whose production is affected by technological limitations related to the quality of the chosen realization process (i.e. leading to fluctuation in the substrate dielectric permittivity, or consistency in line widths and lengths), that eventually leads to difference between simulated and actual antenna. Besides that, the -20dB bandwidth is B_{-20dB}=14.741MHz around f_0'=2.438GHz, whereas B_{-10dB}=49.249MHz, this is a very selective (narrowband) antenna. To sum up, the array looks barely behaving as expected both in- and out-of-band, this must be confirmed by measurements though.

Far field radiation pattern The radiation pattern (with cuts) and the axial ratio are depicted in figures from 18 to 21. These pictures confirm that we have a broadside array (expected, since the radiators are positioned along the x-axis). The ground plane and the beam forming network presence distort the pattern, preventing the array to radiate along negative y-axis tilting the main lobe and directing the maximum radiation along ($\theta = -13°$,$\varphi = 90°$). Moreover, from figure 19 we notice that the antenna is fully linearly polarized at least within the (y,z) plane (since the patch is single-edge fed this is a expected too).

HPBW and SLL From figure 21b,c one has HPBW = 20.4° and SLL=-20.7dB within the (y,z) plane.

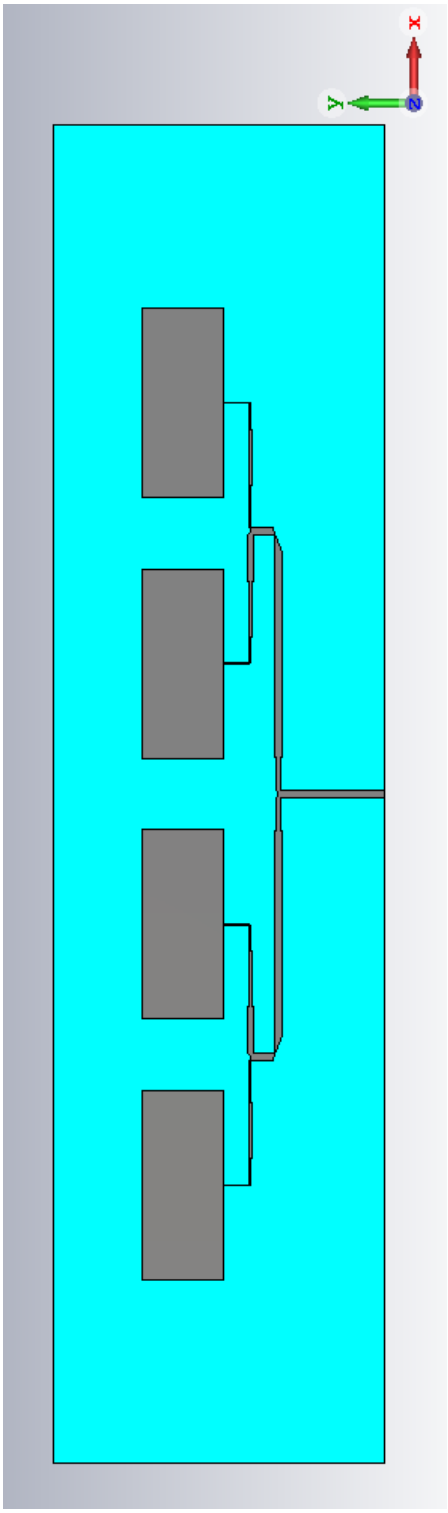

Figure 16: Full array top view, (x,y) plane.

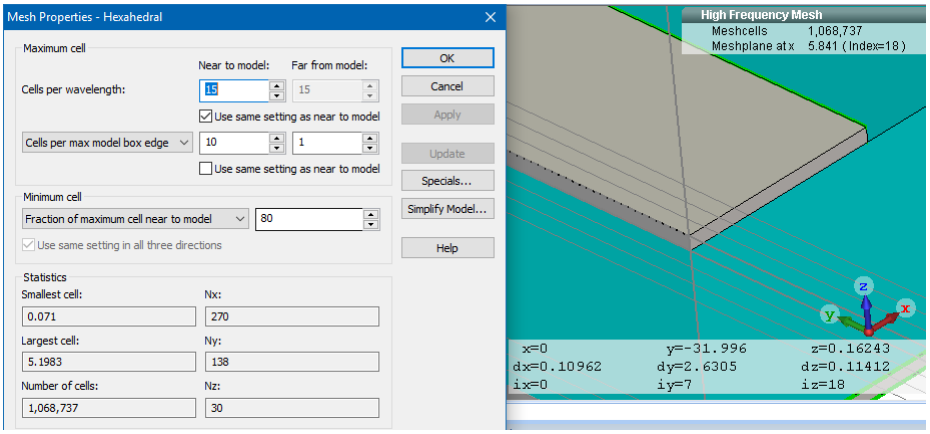

(a) *General settings*

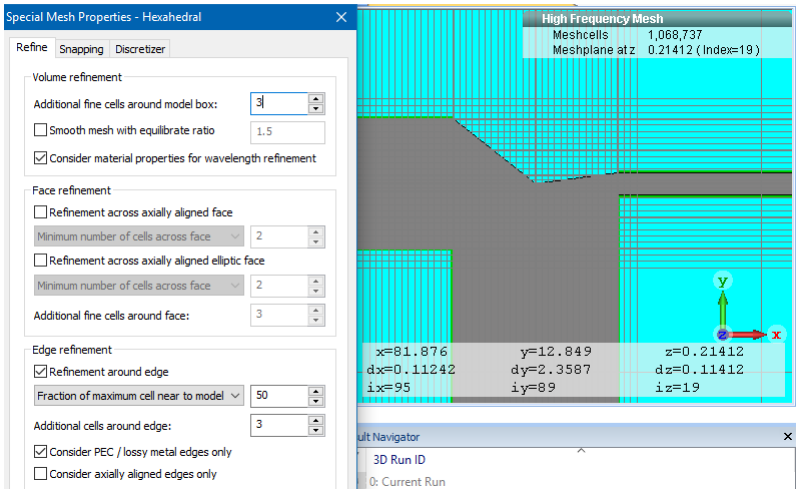

(b) *Special settings*

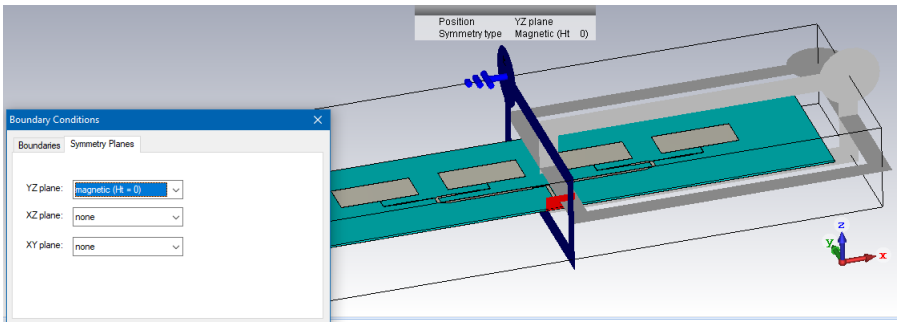

(c) *Boundary conditions: symmetry plane*

Figure 17: Mesh general and special settings. As it appears the mesh has been increased to fit all the bends and narrower lines the best way.

.

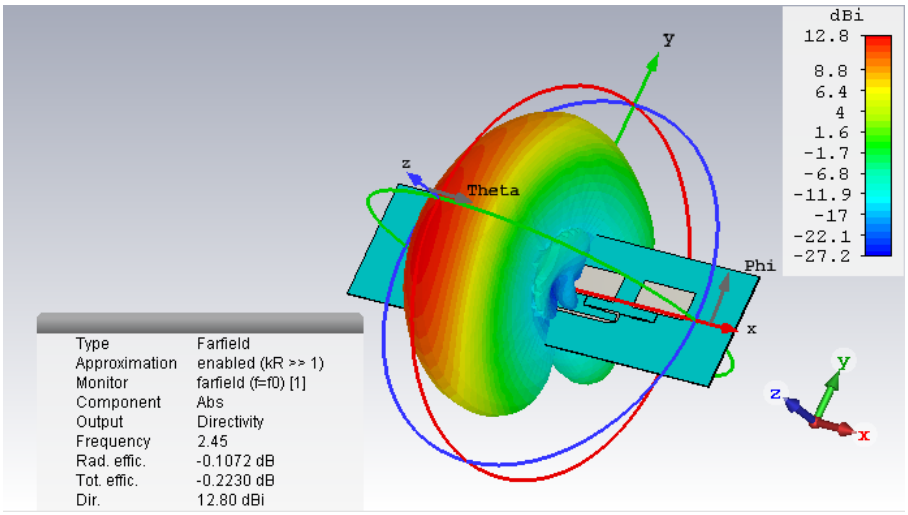

Figure 18: 3D far field radiation pattern.

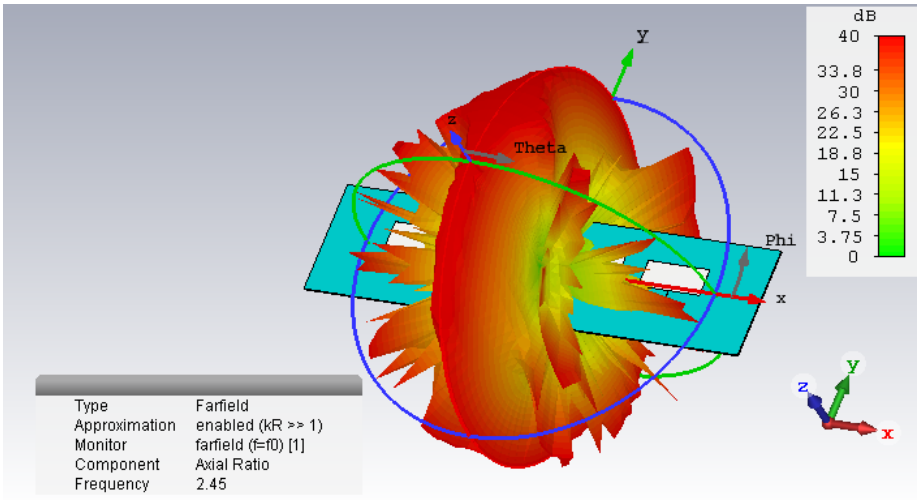

Figure 19: Far field axial ratio.

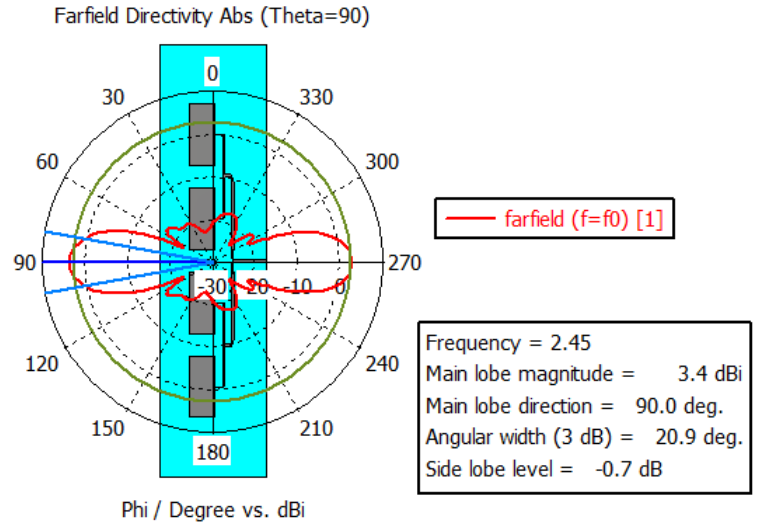

(a) *(x,y) plane cut,* $\theta = 0°$

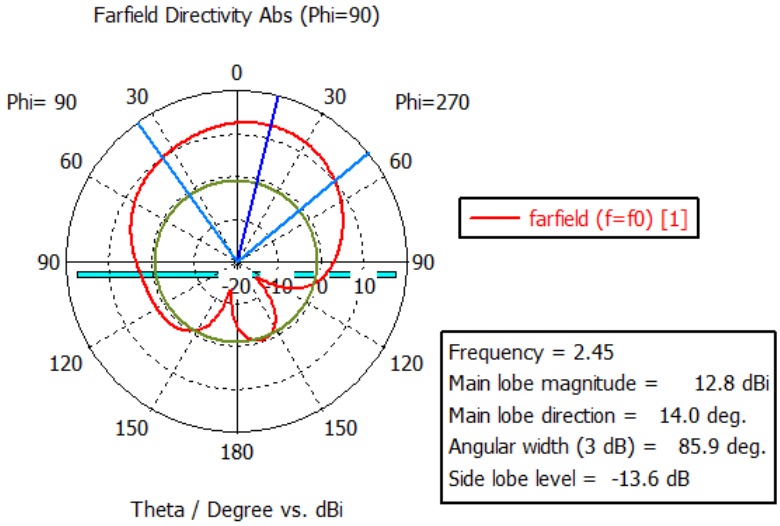

(b) *(y,z) plane cut,* $\varphi = 0°$

Figure 20: Radiation pattern's directivity polar cut planes. As it appears the array radiates broadside within the (y,z) plane. The radiation is minimum along the negative y-direction.

.

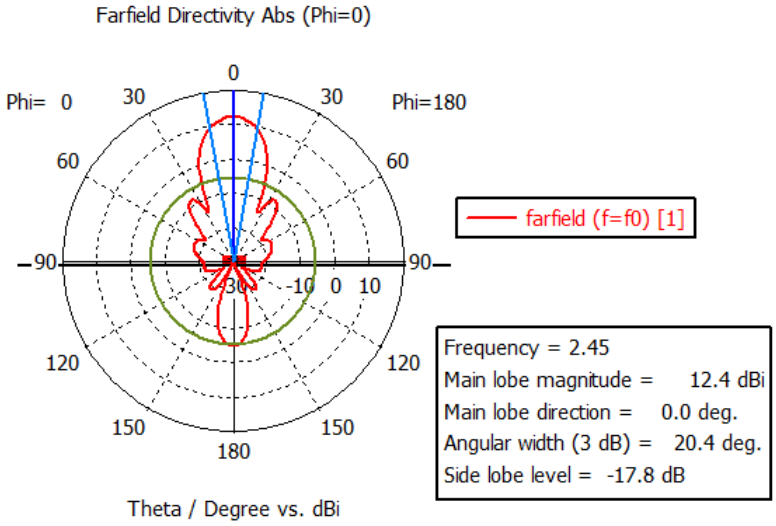

(a) *(x,z) plane polar cut,*$\varphi = 0°$

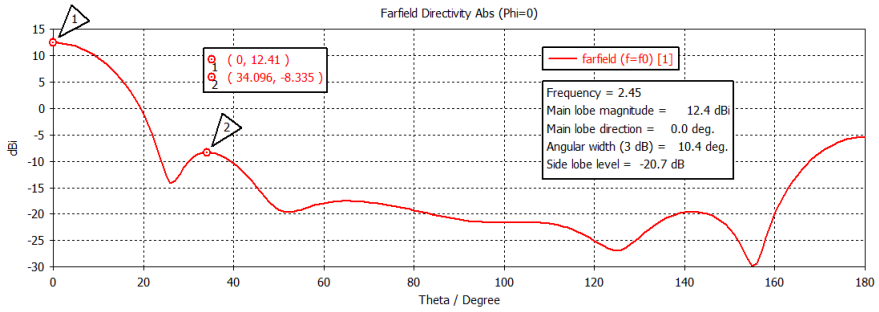

(b) *(x,z) plane cartesian view,* $\varphi = 0°$

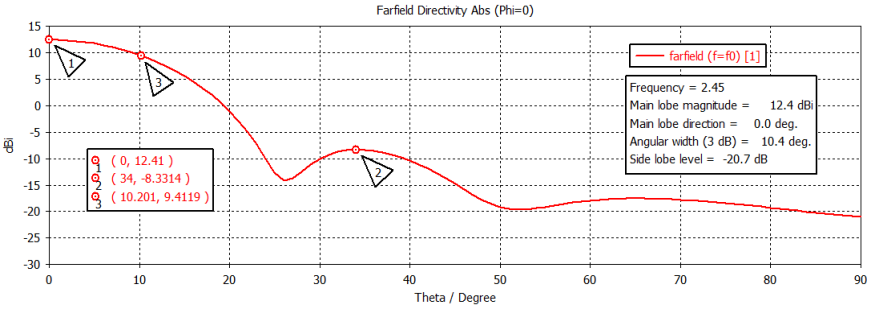

(c) *positive (x,z) plane cartesian view,* $\varphi = 0°$

Figure 21: Radiation pattern's cut planes. As it appears the array radiates broadside within the (y,z) plane. The side lobes level limit is fulfilled, HPBW=20.4°.

.